

**EXPERIMENTAL CHARACTERIZATION AND TWO-ZONE
GLOBAL MODELING OF ECR PRODUCED HYDROGEN
PLASMA FOR MODERATELY LARGE VOLUME
APPLICATIONS**

PRITI SINGH



**DEPARTMENT OF ENERGY SCIENCE AND ENGINEERING
INDIAN INSTITUTE OF TECHNOLOGY DELHI
FEBRUARY 2024**

@ Indian Institute of Technology Delhi (IITD), New Delhi, 2024

**EXPERIMENTAL CHARACTERIZATION AND TWO-ZONE
GLOBAL MODELING OF ECR PRODUCED HYDROGEN
PLASMA FOR MODERATELY LARGE VOLUME
APPLICATIONS**

by

Priti Singh

Department of Energy Science and Engineering

Submitted

in fulfillment of the requirements for the degree of Doctor of Philosophy



to the

Indian Institute of Technology Delhi

February 2024

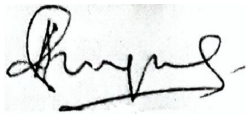
Dedicated to...

...My Loving Son...

...Shreyansh...

CERTIFICATE

This is to certify that the thesis entitled, “**Experimental Characterization and Two-Zone Global Modeling of ECR Produced Hydrogen Plasma for Moderately Large Volume Applications**” submitted by **Ms. Priti Singh**, to the Indian Institute of Technology, Delhi for the award of the degree of **Doctor of Philosophy**, is a bonafide record of the research work done by her under our supervision. The contents of this thesis, in full or in parts, have not been submitted to any other Institute or University for the award of any degree or diploma.



Prof. A. Ganguli

Dept. Energy Science and Engineering
IIT Delhi, New Delhi – 110016
India

Prof. R. Narayanan

Dept. Energy Science and Engineering
IIT Delhi, New Delhi –110016
India

ACKNOWLEDGEMENTS

The accomplishment of this thesis could not have been imaginable without the support of many individuals. I would like to extend my sincere thanks to all the individuals for their consistent help throughout this journey.

Foremost, I would like to start with the person who made the biggest difference in my life, my Ph.D. supervisor **Prof. Ashish Ganguli**. I am extremely obliged to **Prof. Ganguli** for his kind supervision, invaluable persistence, and continuous support during my Ph.D. study. His passion for experimental and theoretical physics was immensely helpful in moving my research work forward. He always inspired me to perform in difficult situations. I am thankful to him for giving me a home in his lab and support over the years. His judgements of living every moment as it comes, making unforeseen surveillance and interpreting them to new possibilities, that will always guide me in future.

It seems impossible to express my gratitude to my Ph.D. supervisor **Prof. Ramesh Narayanan** for his valuable and insightful guidance without which this thesis would have been just a dream. His knowledge and time to time suggestion facilitated me through all the stages of my Ph.D. and helped me to complete my thesis. My special thanks to him for his constant motivation and support throughout my Ph.D. duration.

I would like to extend my sincere thanks to **Prof. R. D. Tarey**, who helped me in designing and fabricating various diagnostics for this thesis work. I would also like to give my heartfelt gratitude to **Prof. Debaprasad Sahu** to help me in simulation of

magnetic fields and global model calculations. I would also like to give my gratitude to **Prof. Satyananda Kar** and **Prof. Bibhuti Bhusan Sahu** for their suggestions and encouragement during the work.

My sincere and special thanks to **Mr. A. J. Josekutty** for giving his valuable time and suggestions during planning of experiments. Without his kind support it was very difficult to conduct the experiments. I would like to give my deepest gratitude to the technical staff of Plasma Lab **Mr. Hasmukh Khabariya** and **Mr. Sumit Lohan** for taking their help during experiments at various stages.

I would like to thank my friends and lab members: **Anshu Verma, Arti Rawat, Prashant Kumar Barnwal, Shweta Sharma, Mahreen** and **Aishik Basu Mallick**, without their support this feat was much more difficult. Thank you all for their unwavering support in tough times and for prompting me to take breaks when I have been stressed out. I am also obliged to **Dr. G. Veda Prakash** for his encouragement and sharing his research expertise during the work. I would also like to give my kind regards to all the members of plasma lab: **Bibekananda, Surajit, Anuravi and Pragya** for their love and support. I would like to thank **Neethu** for taking her help in 3-D topology simulation.

I would like to express my sincere gratitude to **Prof. P. K. Kaw, Prof. A. Chakraborty, Prof. M. Bandyopadhyay** and **Prof. M. Singh** from Institute for Plasma Research, Gandhinagar, for the fruitful discussions on various aspects related to low pressure hydrogen plasmas.

I would also like to thank **Mr. Sunil Bhogal** from Bhogal Precision Limited and **Mr.**

Birender Sharma from Glass Blowing Lab for the fabrication work and also to **Mr. Ghanshyam Sharma** (Liquid Nitrogen Facility) for the continuous supply of liquid nitrogen. I am extremely grateful to the MHRD, India for the PhD scholarship.

Finally, I would like to thank all the members of my **loving family**. I am momentarily beholden to my **Parents and Parents-in-law** for their love and support. Words can hardly describe my thanks and gratitude to my husband **Ravi** for his understanding and love during this journey of my Ph.D. It was his support and encouragement that made this thesis possible. Thank you for having patience when I was frustrated and thank you to be there every time, I need you to just listen. I would like to thank my son **Shreyansh** who is my inspiration for this work and without his unconditional love, I would not be where I am today.

Priti Singh

ABSTRACT

This thesis focusses on the characterization of electron cyclotron resonance (ECR) based hydrogen plasmas for its potential utility in plasma-based applications. The mechanism of ECR power coupling is well known in literature to be one of the most energy efficient processes for plasma applications. The experiments in this thesis work are undertaken in a cylindrical vacuum chamber (diameter = 48.2 cm, length = 75 cm), called Medium Volume Plasma System (MVPS), with an indigenously developed ECR plasma source mounted onto one end of the cylindrical MVPS chamber. The source section uses two different magnetic field configurations (MF1 and MF2), which are demarcated as Compact ECR Plasma Source (CEPS) and Noncompact ECR Plasma Source (NEPS), with the former having a more complex magnetic field configuration (MF1) than the latter (MF2). It is noted that the utility of developing and characterizing new configurations of hydrogen plasma sources is still of relevance in the current era because, depending on the operating conditions, hydrogen plasma can exist in multiple constituent species of hydrogen (H_2 , H , H^+ , H_2^+ , H_3^+ and H^-) with varying ratios which enables it to be used for a wide array of applications in various fields of science and technology *viz.*, impurity removal from metals, passivation of semiconductor material, enhancement of growth rate of diamond films and surface treatment to protect from corrosive effects, plasma ion implantation and hydrogenation of polysilicon thin-film transistors, ion projection lithography and neutral beam injection (NBI) system for fusion devices to name a few.

This extensive range of hydrogen plasma applications along with some recent experiments using the patented CEPS, developed by the Plasma Lab at IIT Delhi, which has demonstrated the CEPS to be a generic source suitable for various applications provided a motivation for the work on ECR-based hydrogen plasmas using the CEPS and NEPS carried out in this thesis. The CEPS is a permanent magnet based ECR plasma source weighing only about ≈ 14 kgs (including the NdFeB permanent ring magnets), with length ≈ 60 cm and comprises of the waveguide microwave launcher, dual directional coupler (for forward and reflected power measurement), triple stub impedance matching unit, rectangular-to-circular waveguide transition and the plasma source section (PSS) all integrated into a single unit. Both the CEPS and the NEPS use the same microwave line except for the set of NdFeB permanent ring magnets of the CEPS being replaced by another combination of NdFeB permanent ring magnets and electromagnet coils in the NEPS. The magnetic field configuration (MF1) of CEPS as well as the alternate or second magnetic field configuration (MF2) of NEPS generate suitable ECR fields within the PSS but which are still distinctly *different* from each other.

A series of experiments were performed for different operating parameters in both magnetic field configurations. The primary diagnostics used in this work are a set of radial and axial Langmuir Probe (LP) along with a Retarding Field Energy Analyser (RFEA); all diagnostics being fabricated in-house. The axial LP data for MF1 were recorded from $z \approx 4$ cm to $z \approx 50$ cm, measured from the source mouth, due to the complex field configuration of MF1. It may be mentioned that *two electron populations* are always present in the expansion chamber (*i.e.* for $z \geq 4$ cm) in MF1: a *high density bulk population* (n) with a *low electron temperature* (T_e) and a *low density warm population* ($n_w \ll n$) with *relatively high electron temperature* ($T_w \gg T_e$). LP measurements reveal high-density hydrogen plasma ($\approx 10^{11}$ cm⁻³), with high bulk electron temperatures ($T_e \approx 8$ eV) and plasma potentials ($V_p \approx 50$ V) at very modest microwave power ($P \approx 600$ W) over a wide range of pressures ($p \approx 1$ to 8 mTorr) close to the

source mouth. Ion energy analysis using RFEA shows nearly mono-energetic ion beams with beam energy $E_b \approx 98$ eV in front of the CEPS at 1mTorr pressure. As pressure increases, the ion beam energy decreases, such that at 8 mTorr the ion beam energy is $E_b \approx 17$ eV in front of CEPS.

One the other hand, due to the less harsh environment in MF2 one is able to probe deeper in to the source which reveals that the plasma starts with a *single* electron population originally and later splits into two electron population with the low temperature, bulk electron population showing a relative density enhancement than that observed upstream before the onset of splitting and is also co-existing with a higher temperature but relatively lower density warm electron population. The point at which splitting occurs can vary from well inside the source to outside the source. LP measurements reveal high-density hydrogen plasma ($n \approx 10^{11}$ cm⁻³), with high bulk electron temperatures ($T_e \approx 7$ eV) and plasma potentials ($V_p \approx 30$ V) at microwave power ($P \approx 650$ W) over a wide range of pressures ($p \approx 1$ to 8 mTorr) in front of NEPS in the expansion chamber. One also observes a significant drop within the source near to the exit and the resulting ambipolar field help to accelerate the escaping ions from the PSS. RFEA also shows nearly mono-energetic ions with beam energy $E_b \approx 63$ eV, in front of the source at 1 mTorr pressure. As pressure increases the measured energy of the ion beam decreases, such that at 8 mTorr, $E_b \approx 7$ eV in front of the NEPS mouth.

Based on the results obtained from the experiments undertaken with NEPS, a model is proposed to explain the observation of a transition from a single-to-two electron population. The model identifies that the resonating electrons gain energy from the ECR field and then traverses a distance of a few meters, equivalent to the electron-neutral ionization mean free path (λ_{en}), along a helical trajectory but is effectively displaced from the ECR layer only by a distance of a few centimeters towards the expansion chamber. This displacement has been found to be well correlated with the distance from the ECR layer to the point of splitting,

suggesting this to be the distance that is required for the energetic electrons emanating from the ECR zone to trigger an avalanche ionization process. Thereafter the bulk density is found to follow a n/B scaling initially for about 4-5 cms and then the density is found to decay much slower than that of the magnetic field. This scaling has been identified to be the distance over which the parallel diffusion coefficient (D_{\parallel}) is significantly dominant over the perpendicular diffusion coefficient (D_{\perp}). The proposed model was also able to provide an insight into the mechanism of the plasma generation within the CEPS and provide the plausible reason for generation of such high plasma potential drops across or near to the source mouth that explains the observation of relatively higher ion beam energies, making it a very harsh environment for probe studies.

In order to predict the presence of ion beams in the expansion chamber and to describe the plasma behaviour in expanding geometry, an unmagnetized, zero dimensional, 2-zone global model has been developed where zone-1 and zone-2 represent the source section and expansion chamber respectively. Separate particle and power balance equations were setup for the two zones that take into account particle and power flow across the two zones, wall losses, current balance across the interconnecting opening, etc. The results of the two zone global model obtained in this thesis are compared with the experimental results both inside and outside the source of the NEPS and are found to have a reasonable match between them. The unmagnetized zero-dimensional model was also able to predict the presence of a potential jump in the expanding field geometry. This implies that the expanding geometry contributes to the generation of potential drops across the source mouth which can be further enhanced by suitable tuning of the magnetic field configuration within the PSS leading to potential applications in the near future. The details of these investigations and inferences are presented in this thesis work.

सारांश

यह थीसिस प्लाज्मा आधारित अनुप्रयोगों में इसकी संभावित उपयोगिता के लिए इलेक्ट्रॉन साइक्लोट्रॉन अनुनाद (ईसीआर) आधारित हाइड्रोजन प्लाज्मा के लक्षण वर्णन पर केंद्रित है। ईसीआर पावर कपलिंग का तंत्र साहित्य में प्लाज्मा अनुप्रयोगों के लिए सबसे अधिक ऊर्जा कुशल प्रक्रियाओं में से एक होने के लिए जाना जाता है। इस शोध कार्य में प्रयोग एक बेलनाकार निर्वात कक्ष (व्यास = 48.2 सेमी, लंबाई = 75 सेमी) में किए जाते हैं, जिसे मध्यम आयतन प्लाज्मा सिस्टम (एमवीपीएस) कहा जाता है, जिसमें बेलनाकार एमवीपीएस कक्ष के एक छोर पर स्वदेशी रूप से विकसित ईसीआर प्लाज्मा स्रोत लगा होता है। . स्रोत खंड दो अलग-अलग चुंबकीय क्षेत्र विन्यास (एमएफ1 और एमएफ2) का उपयोग करता है, जिन्हें कॉम्पैक्ट ईसीआर प्लाज्मा स्रोत (सीईपीएस) और नॉनकॉम्पैक्ट ईसीआर प्लाज्मा स्रोत (एनईपीएस) के रूप में सीमांकित किया जाता है, जिसमें पूर्व में अधिक जटिल चुंबकीय क्षेत्र विन्यास (एमएफ1) होता है। बाद वाला (एमएफ 2)। यह नोट किया जाता है कि हाइड्रोजन प्लाज्मा स्रोतों के नए विन्यासों के विकास और लक्षण वर्णन की उपयोगिता वर्तमान युग में अभी भी प्रासंगिक है, क्योंकि परिचालन स्थितियों के आधार पर, हाइड्रोजन प्लाज्मा हाइड्रोजन की कई घटक प्रजातियों (H_2 , H , H^+ , H_2^+) में मौजूद हो सकता है। , H_3^+ और H^-) अलग-अलग अनुपातों के साथ जो इसे

विज्ञान और प्रौद्योगिकी के विभिन्न क्षेत्रों में अनुप्रयोगों की एक विस्तृत श्रृंखला के लिए उपयोग करने में सक्षम बनाता है। संक्षारक प्रभावों से बचाने के लिए उपचार, पॉलीसिलिकॉन पतली-फिल्म ट्रांजिस्टर के प्लाज्मा आयन आरोपण और हाइड्रोजनीकरण, संलयन उपकरणों के लिए आयन प्रक्षेपण लिथोग्राफी और तटस्थ बीम इंजेक्शन (एनबीआई) प्रणाली कुछ नाम हैं।

IIT दिल्ली में प्लाज्मा लैब द्वारा विकसित पेटेंट CEPS का उपयोग करते हुए कुछ हालिया प्रयोगों के साथ-साथ हाइड्रोजन प्लाज्मा अनुप्रयोगों की यह विस्तृत श्रृंखला, जिसने CEPS को विभिन्न अनुप्रयोगों के लिए उपयुक्त एक सामान्य स्रोत के रूप में प्रदर्शित किया है, ने ECR-आधारित कार्य के लिए प्रेरणा प्रदान की है। इस थीसिस में किए गए CEPS और NEPS का उपयोग कर हाइड्रोजन प्लाज्मा। CEPS एक स्थायी चुंबक आधारित ECR प्लाज्मा स्रोत है, जिसका वजन केवल ≈ 14 किलोग्राम (NdFeB स्थायी रिंग मैग्नेट सहित) है, जिसकी लंबाई ≈ 60 सेमी है और इसमें वेवगाइड माइक्रोवेव लॉन्चर, डुअल डायरेक्शनल कपलर (आगे और परावर्तित शक्ति माप के लिए) शामिल हैं। ट्रिपल स्टब प्रतिबाधा मिलान इकाई, आयताकार-से-परिपत्र वेवगाइड संक्रमण और प्लाज्मा स्रोत अनुभाग (PSS) सभी एक इकाई में एकीकृत हैं। CEPS के NdFeB स्थायी रिंग मैग्नेट के सेट को छोड़कर CEPS और NEPS दोनों एक ही माइक्रोवेव लाइन का उपयोग करते हैं, जिसे NEPS में NdFeB स्थायी रिंग मैग्नेट और इलेक्ट्रोमैग्नेट कॉइल के दूसरे संयोजन द्वारा प्रतिस्थापित किया जाता है। CEPS के चुंबकीय क्षेत्र विन्यास (MF1)

के साथ-साथ NEPS के वैकल्पिक या दूसरे चुंबकीय क्षेत्र विन्यास (MF2) PSS के भीतर उपयुक्त ECR क्षेत्र उत्पन्न करते हैं लेकिन जो अभी भी एक दूसरे से अलग हैं।

दोनों चुंबकीय क्षेत्र विन्यासों में विभिन्न ऑपरेटिंग मापदंडों के लिए प्रयोगों की एक श्रृंखला का प्रदर्शन किया गया। इस कार्य में उपयोग किए जाने वाले प्राथमिक निदान रेडियल और अक्षीय लेंगमुइर प्रोब (एलपी) के साथ-साथ एक रिटार्डिंग फील्ड एनर्जी एनालाइज़र (आरएफईए) का एक सेट है; सभी डायग्नोस्टिक्स इन-हाउस गढ़े जा रहे हैं। MF1 के जटिल क्षेत्र विन्यास के कारण, MF1 के लिए अक्षीय LP डेटा $z \approx 4$ सेमी से $z \approx 50$ सेमी, स्रोत मुंह से मापा गया था। यह उल्लेख किया जा सकता है कि एमएफ1 में दो इलेक्ट्रॉन आबादी हमेशा विस्तार कक्ष (यानी जेड ≥ 4 सेमी के लिए) में मौजूद होती है: एक उच्च घनत्व थोक आबादी (एन) कम इलेक्ट्रॉन तापमान (टीई) और कम घनत्व गर्म आबादी (एनडब्ल्यू) के साथ $\ll n$) अपेक्षाकृत उच्च इलेक्ट्रॉन तापमान ($T_w \gg T_e$) के साथ। एलपी माप उच्च-घनत्व वाले हाइड्रोजन प्लाज्मा ($\approx 10^{11}$ सेमी³) को प्रकट करते हैं, उच्च बल्क इलेक्ट्रॉन तापमान ($T_e \approx 8$ eV) और प्लाज्मा क्षमता ($V_p \approx 50$ V) के साथ बहुत मामूली माइक्रोवेव पावर ($P \approx 600$ W) एक विस्तृत श्रृंखला पर स्रोत के मुंह के करीब दबाव ($p \approx 1$ से 8 mTorr)। RFEA का उपयोग कर आयन ऊर्जा विश्लेषण 1mTorr दबाव पर CEPS के सामने बीम ऊर्जा $E_b \approx 98$ eV के साथ लगभग मोनो-ऊर्जावान आयन बीम दिखाता है। जैसे ही दबाव बढ़ता है, आयन बीम ऊर्जा कम हो जाती है, जैसे कि 8 mTorr पर CEPS के सामने आयन बीम ऊर्जा $E_b \approx 17$ eV है।

दूसरी ओर, एमएफ2 में कम कठोर वातावरण के कारण स्रोत की गहराई से जांच करने में सक्षम है जो बताता है कि प्लाज्मा मूल रूप से एक इलेक्ट्रॉन आबादी के साथ शुरू होता है और बाद में कम तापमान, बल्क इलेक्ट्रॉन आबादी के साथ दो इलेक्ट्रॉन आबादी में विभाजित हो जाता है। बंटवारे की शुरुआत से पहले ऊपर की ओर देखी गई तुलना में एक सापेक्षिक घनत्व वृद्धि दिखा रहा है और यह उच्च तापमान के साथ सह-अस्तित्व में है, लेकिन अपेक्षाकृत कम घनत्व वाली गर्म इलेक्ट्रॉन आबादी है। जिस बिंदु पर विभाजन होता है, वह स्रोत के अंदर अच्छी तरह से स्रोत के बाहर भिन्न हो सकता है। . एलपी माप उच्च घनत्व वाले हाइड्रोजन प्लाज्मा ($n \approx 10^{11}$ सेमी³) को उच्च बल्क इलेक्ट्रॉन तापमान ($T_e \approx 7$ eV) और प्लाज्मा क्षमता ($V_p \approx 30$ V) के साथ माइक्रोवेव पावर ($P \approx 650$ W) पर एक विस्तृत श्रृंखला में प्रकट करते हैं। विस्तार कक्ष में NEPS के सामने दबाव ($p \approx 1$ से 8 mTorr)। बाहर निकलने के करीब स्रोत के भीतर एक महत्वपूर्ण गिरावट भी देखी जाती है और परिणामी एंबिपोलर क्षेत्र पीएसएस से भागने वाले आयनों को तेज करने में मदद करता है। RFEA 1 mTorr दबाव पर स्रोत के सामने बीम ऊर्जा $E_b \approx 63$ eV के साथ लगभग मोनो-ऊर्जावान आयन भी दिखाता है। जैसे ही दबाव बढ़ता है, आयन बीम की मापी गई ऊर्जा कम हो जाती है, जैसे कि 8 mTorr पर, NEPS मुंह के सामने $E_b \approx 7$ eV.

एनईपीएस के साथ किए गए प्रयोगों से प्राप्त परिणामों के आधार पर, एक-से-दो इलेक्ट्रॉन आबादी से संक्रमण के अवलोकन की व्याख्या करने के लिए एक मॉडल प्रस्तावित

है। मॉडल की पहचान है कि प्रतिध्वनित इलेक्ट्रॉन ईसीआर क्षेत्र से ऊर्जा प्राप्त करते हैं और फिर कुछ मीटर की दूरी तय करते हैं, इलेक्ट्रॉन-तटस्थ आयनीकरण के बराबर मुक्त पथ (λ_{en}), एक पेचदार प्रक्षेपवक्र के साथ लेकिन केवल ईसीआर परत से प्रभावी रूप से विस्थापित होता है विस्तार कक्ष की ओर कुछ सेंटीमीटर की दूरी से। इस विस्थापन को ईसीआर परत से बंटवारे के बिंदु तक की दूरी के साथ अच्छी तरह से सहसंबद्ध पाया गया है, यह सुझाव देता है कि यह वह दूरी है जो ईसीआर क्षेत्र से निकलने वाले ऊर्जावान इलेक्ट्रॉनों के लिए हिमस्खलन आयनीकरण प्रक्रिया को ट्रिगर करने के लिए आवश्यक है। तत्पश्चात बल्क घनत्व लगभग 4-5 सेमी के लिए शुरू में n/B स्केलिंग का पालन करने के लिए पाया जाता है और फिर घनत्व चुंबकीय क्षेत्र की तुलना में बहुत धीमी गति से क्षय पाया जाता है। इस स्केलिंग की पहचान उस दूरी के रूप में की गई है जिस पर समांतर प्रसार गुणांक ($Z_{||}$) लंबवत प्रसार गुणांक (Z_{\perp}) पर महत्वपूर्ण रूप से प्रभावी है। प्रस्तावित मॉडल सीईपीएस के भीतर प्लाज्मा पीढ़ी के तंत्र में एक अंतर्दृष्टि प्रदान करने में भी सक्षम था और स्रोत मुंह के पास या उसके पास ऐसी उच्च प्लाज्मा संभावित बूंदों की पीढ़ी के लिए प्रशंसनीय कारण प्रदान करता है जो अपेक्षाकृत उच्च आयन बीम ऊर्जा के अवलोकन की व्याख्या करता है। , जांच अध्ययन के लिए यह बहुत कठोर वातावरण बनाता है।

विस्तार कक्ष में आयन बीम की उपस्थिति की भविष्यवाणी करने के लिए और विस्तारित ज्यामिति में प्लाज्मा व्यवहार का वर्णन करने के लिए, एक अचुम्बकीय, शून्य

आयामी, 2-ज़ोन वैश्विक मॉडल विकसित किया गया है जहाँ ज़ोन -1 और ज़ोन -2 स्रोत खंड का प्रतिनिधित्व करते हैं और विस्तार कक्ष क्रमशः। दो ज़ोन के लिए अलग-अलग कण और शक्ति संतुलन समीकरण स्थापित किए गए थे जो दो ज़ोन में कण और बिजली के प्रवाह, दीवार के नुकसान, इंटरकनेक्टिंग ओपनिंग में वर्तमान संतुलन आदि को ध्यान में रखते हैं। इस थीसिस में प्राप्त दो ज़ोन वैश्विक मॉडल के परिणाम हैं एनईपीएस के स्रोत के अंदर और बाहर दोनों प्रायोगिक परिणामों की तुलना में और उनके बीच एक उचित मेल पाया जाता है। अचुंबकीय शून्य-आयामी मॉडल विस्तारित क्षेत्र ज्यामिति में संभावित उछाल की उपस्थिति की भविष्यवाणी करने में भी सक्षम था। इसका तात्पर्य यह है कि विस्तारित ज्यामिति स्रोत मुंह में संभावित बूंदों की पीढ़ी में योगदान देती है जिसे निकट भविष्य में संभावित अनुप्रयोगों के लिए पीएसएस के भीतर चुंबकीय क्षेत्र विन्यास के उपयुक्त ट्यूनिंग द्वारा बढ़ाया जा सकता है। इस शोध कार्य में इन जांचों और अनुमानों का विवरण प्रस्तुत किया गया है।

Contents

Certificate	(i)
Acknowledgment	(iii)
Abstract	(vii)
List of Figures.....	(xxi)
List of Tables	(xxvii)
1. Introduction.....	1
1.1 Introduction to Hydrogen Plasma	1
1.2 Motivation aspects	3
1.3 Literature Review on Hydrogen Plasma Sources and Applications.....	7
1.4 Objectives of the thesis.....	16
1.5 Methodology.....	18
1.6 Summary of the research work.....	20
1.7 Highlights of the thesis.....	21
References.....	27
2. Experimental Setup and Diagnostics.....	39
2.1 Introduction.....	39

2.2 The CEPS and the NEPS.....	42
2.3 Medium Volume Plasma System (MVPS).....	45
2.4 Diagnostics.....	47
2.4.1 Langmuir Probes.....	47
2.4.2 Retarding Field Energy Analyzer (RFEA) for Ions.....	58
References	65
3. Characterization of Plasma Produced by CEPS within MVPS.....	69
3.1 Introduction	69
3.2 MF1 – The CEPS Magnetic Field.....	70
3.3 Plasma Characterization Results.....	80
3.3.1 Axial Langmuir Probe Results.....	82
3.3.2 Radial Langmuir Probe Results.....	88
3.3.3 Analysis of electron expansion in MVPS.....	90
3.3.4 RFEA Results.....	92
3.4 Summary.....	97
References.. ..	98
4. Characterization of Plasma Produced by NEPS within MVPS.....	101
4.1 Introduction	101
4.2 MF2- The NEPS Magnetic Field.....	102
4.3 Plasma Characterization Results.....	104

4.3.1 Axial Langmuir Probe Results.....	105
4.3.2 Analysis of the region of splitting of electron population.....	111
4.3.3. Radial Langmuir Probe Results.....	124
4.3.4 Analysis of electron expansion in MVPS.....	127
4.3.5 RFEA Results.....	129
4.4 Comparative Analysis of CEPS and NEPS.....	133
4.5 Summary.....	142
References.	147
5. Development of Two-Zone Global Model and Validation of the Experimental Result for NEPS.....	151
5.1 Introduction..	151
5.2 Steady State 2-Zone Global Model for Vetting Plasma Parameters in MVPS.....	153
5.3 The Equations Involved in the Model.....	158
5.4 Model Validation and Comparison with Experiments.....	162
5.5 Summary.....	166
References.....	169
6. Conclusion and Future Scope.....	171
6.1 Summary.....	171
6.2 Future Scope.....	175
List of Publications.....	177

List of Figures

Figure 1.1 Application of Hydrogen Plasma in different fields.....	2
Figure 1.2 (a) The schematic representation of CEPS; (b) Medium Volume Plasma system (MVPS); (c) Large Volume Plasma System (LVPS).....	5
Figure 1.3 RF plasma system for etching of semiconductors.....	11
Figure 1.4 (a) Positive ion population dominating in Hydrogen plasma at 0.4 Pa, 100 W; (b) Positive ion population dominating in Hydrogen plasma at 1 Pa, 50 W.....	13
Figure 2.1 (a) Schematic of the essential components of the ECR plasma source used in CEPS; (b) Axial magnetic field profile of MF1 (CEPS) and (c) Axial magnetic field profile of MF2 (NEPS).....	42
Figure 2.2 Schematic of MVPS showing mounting of the PSS for the CEPS / NEPS and the location of ports for various diagnostics.....	46
Figure 2.3 Schematic of (a) magnet for MF1 and (b) magnet and coil for MF2.....	46
Figure 2.4 Schematic of Radial Langmuir probe.....	48
Figure 2.5 Schematic of Axial Langmuir probe.....	48
Figure 2.6 (a) Typical I - V characteristic of axial LP obtained at $z = - 4$ cm (inside PSS) for hydrogen plasma at ~ 3 mTorr, 650 W.	54
Figure 2.7 (a) Typical I - V characteristic of axial LP obtained at $z = 45$ cm (inside expansion chamber) for hydrogen plasma at ~ 3 mTorr, 650 W.	54
Figure 2.8 The Retarding Field Analyzer (RFEA): (a) schematic of the RFEA and (b) The grid biasing layout used in the RFEA (for both CEPS and NEPS) where the acronyms signify ER: Electron Repeller, ID: Ion Discriminator, ES: Secondary Electron Suppressor, C: Collector.....	59

Figure 2.9 (a) I_c-V_d characteristics measured using the RFEA positioned at $z = 5$ and 10 cm in front of PSS for 1 mTorr hydrogen pressure and microwave power of 650 W (for NEPS); (b) the first derivative of I_c-V_d . and (c) the ion energy distribution function $f(E)$ with respect to E derived from the I_c-V_d characteristics of RFEA.....	63
Figure 3.1 Schematic of the essential components of compact ECR plasma source (CEPS).....	70
Figure 3.2 (a) MF1 field configuration for CEPS: Detailed view of magnetic field inside the PSS. The coloured lines indicate the contours of constant magnetic field and the dashed lines, the magnetic field lines; (b) Axial magnetic field profile inside the PSS and the MVPS; (c) The field lines and contours of constant magnetic field inside the PSS and the MVPS.....	71
Figure 3.3 (a) Magnetic flux density close to z axis in MF1; (b) zoomed plot of highlighted rectangular portion (dashed magenta) in fig 3.3(a).....	74
Figure 3.4 3D-topology of selected magnetic field lines (in fig. 3.3) of the CEPS (MF1).....	75
Figure 3.5 (a) Field lines of a magnetic mirror in linear configuration; (b) Magnetic field profile of a typical mirror profile showing particle trajectory of a trapped particle in linear geometry.....	76
Figure 3.6 (a) 3D-topology of NEPS (MF2); (b) Detailed view of magnetic field configuration in MF2: The coloured lines indicate the contours of constant magnetic field intensity and the dashed lines are the magnetic field lines.....	78
Figure 3.7 Axial profile of hydrogen plasma parameters at different pressures using 650 W microwave power. (a) 1 mTorr; (b) 2 mTorr; (c) 3 mTorr; (i) bulk electron density (n); (ii) warm electron density (n_w); (iii) bulk electron temperature (T_e); (iv) warm electron temperature (T_w) and (v) plasma potential (V_p).	83
Figure 3.8 Axial profile of hydrogen plasma parameters at different pressures using 650 W microwave power. (a) 6 mTorr; (b) 8 mTorr; (i) bulk electron density (n); (ii) warm electron density (n_w); (iii) bulk electron temperature (T_e); (iv) warm electron temperature (T_w) and (v) plasma potential (V_p).	84

- Figure 3.9 Normalized axial hydrogen plasma density profile at different pressures with 650 W microwave power input: $p = 1$ mTorr [red solid circles]; 2 mTorr [brown solid triangle]; 3 mTorr [blue closed square]; 6mTorr [magenta open circle]; 8mTorr [green open squares]. The plasma density and magnetic field has been normalized with respect to their values at $z = 4$ cm.....86
- Figure 3.10 Radial profiles of hydrogen plasma parameters at different pressures using 650 W microwave power at axial locations R_1 and R_2 , corresponding to $z \approx 13.8$ cm and ≈ 38.8 cm respectively. (a) 1 mTorr; (b) 8 mTorr; (i) bulk electron density (n); (ii) warm electron density (n_w); (iii) bulk electron temperature (T_e); (iv) warm electron temperature (T_w) and (v) plasma potential (V_p).....88
- Figure 3.11 Polytropic relation obtained from experimental data (a) 1 mTorr; (b) 2 mTorr; (c) 6 mTorr and (d)8 mTorr using microwave power ≈ 650 W.....90
- Figure 3.12 Collector current, I_c versus discriminator voltage, V_d characteristics measured using the RFEA at axial positions, $z \approx 10$ and 5 cm for pressures, (a) 1 mTorr; (b) 2 mTorr; (c) 3 mTorr and (d) 8 mTorr and microwave power ≈ 650 W.....92
- Figure 3.13 The ion energy distribution function $f(E)$ with respect to E derived from the RFEA characteristics given in Figure. 3.12. (a) 1 mTorr; (b) 2 mTorr pressure and microwave power of 650 W.....94
- Figure 3.14 The ion energy distribution function $f(E)$ with respect to E derived from the RFEA characteristics given in Figure. 3.12. (a) 3 mTorr; (b) 8 mTorr pressure and microwave power of 650 W.....95
- Figure 4.1 Schematic of details of MF2.....103
- Figure 4.2 Detailed view of magnetic field configuration in MF2. (a) The magnetic field configuration inside the source section The coloured lines indicate the contours of constant magnetic field intensity and the dashed lines are the magnetic field lines; (b) The monotonically varying axial magnetic field profile of MF2 configuration; (c) The magnetic field lines and contours of constant magnetic field intensity are shown.....104
- Figure 4.3. Axial profile of hydrogen plasma parameters obtained using 650 W microwave input power at different pressures: (a) 1 mTorr; (b) 2 mTorr; (c) 3 mTorr. The plasma parameters in each subplot are (i) bulk electron density (n); (ii) warm electron density (n_w); (iii) bulk electron temperature (T_e); (iv) warm electron

temperature (T_w) and (v) plasma potential (V_p). The location of the splitting is marked as a dashed vertical line.....108

Figure 4.4 Axial profile of hydrogen plasma parameters obtained using 650 W microwave input power at different pressures: (a) 6 mTorr; (b) 8 mTorr. The plasma parameters in each subplot are (i) bulk electron density (n); (ii) warm electron density (n_w); (iii) bulk electron temperature (T_e); (iv) warm electron temperature (T_w) and (v) plasma potential (V_p)..109

Figure 4.5 Comparison of the normalized magnetic field with the normalized axial density profile obtained using 650 W microwave input power at different pressures: (a) 1 mTorr; (b) 2 mTorr; (c) 3 mTorr; (d) 6 mTorr; (e) 8mTorr. The normalization is evaluated with reference to the maximum bulk plasma density for each pressure, which is the location at which the splitting occurs (single-electron to two-electron population).....114

Figure 4.6. The axial variation of (a) electron-neutral ionization mean free path (λ_{en}); (b) electron cyclotron gyro-frequency (ω_{ce}); (c) electron Larmor radius (r_{LE});(d) Hydrogen ion-hydrogen neutral (H^+ -H) elastic collision mean free path (λ_{H^+-H}); (e) ion cyclotron gyro-frequency (ω_{ci}); (f) ion Larmor radius (r_{Li}) with $T_i \approx 0.5$ eV, for different pressures.....115

Figure 4.7. The axial variation of (a) parallel diffusion coefficient ($D_{||}$); (b) ratio of ion larmor radius and $H-H^+$ mean free path (c) perpendicular diffusion coefficient (D_{\perp}); (d) ratio of D_{\perp} to $D_{||}$ for different pressures and for ion temperatures $T_i \approx 0.5$ eV.....122

Figure 4.8. Radial profiles of hydrogen plasma parameters at different pressures using 650 W microwave power at axial locations R_1 and R_2 , corresponding to $z \approx 13.8$ cm and ≈ 38.8 cm respectively. (a) 1 mTorr (b) 8 mTorr ; (i) bulk electron density (n); (ii) warm electron density (n_w); (iii) bulk electron temperature (T_e); (iv) warm electron temperature (T_w) and (v) plasma potential (V_p).....125

Figure 4.9. Polytopic relation obtained from experimental data (a) 1 mTorr; (b) 2 mTorr; (c) 6 mTorr and (d) 8 mTorr using microwave power $\gg 650$ W.....128

Figure 4.10 $I_c(V_d)$ characteristics measured using the RFEA positioned at $z = 10$ and 5 cm in front of CEPS for (a) 1 mTorr; (b) 2 mTorr; (c) 3 mTorr and (d) 8 mTorr pressure and microwave power of 650 W.....130

Figure 4.11 The ion energy distribution function $f(E)$ with respect to E derived from the RFEA characteristics given in Fig.4.10. (a) 1 mTorr; (b) 2 mTorr pressure and microwave power of 650 W.....	131
Figure 4.12 The ion energy distribution function $f(E)$ with respect to E derived from the RFEA characteristics given in Fig.4.10. (a) 3 mTorr; (b) 8 mTorr pressure and microwave power of 650 W.....	132
Figure 4.13 Comparison of plasma density for both the configurations (a) MF1 and (b) MF2.....	135
Figure 4.14 Comparison of electron temperature for both the configurations (a) MF1 and (b) MF2.....	135
Figure 4.15 Comparison of plasma potential for both the configurations (a) MF1 and (b) MF2.....	136
Figure 4.16 Comparison of ion energies for both the configurations (a) MF1 and (b) MF2 for $z \approx 5\text{cm}$ and $z \approx 10\text{ cm}$	136
Figure 5.1 Schematic of the 2-Zone global model geometry.....	157
Figure 5.2 Plasma density in Zone-1 and Zone-2, calculated at 650 W microwave power and at various pressure (black diamond) and a comparison with the experimental values (red circle). [a] plasma density (n_1) in Zone-1; [b] plasma density (n_2) in Zone-2.....	164
Figure 5.3 Bulk electron temperature in Zone-1 and Zone-2, calculated at 650 W microwave power and at various pressure (black diamond) and a comparison with the experimental values (red circle). [a] Bulk electron temperature (Te_1) in Zone-1; [b] Bulk electron temperature (Te_2) in Zone-2.....	164
Figure 5.4 Plasma Potential in Zone-1 and Zone-2, calculated at 650 W microwave power and at various pressure (black diamond) and a comparison with the experimental values (red circle). [a] Plasma potential (Vp_1) in Zone-1; [b] Bulk electron temperature (Vp_2) in Zone-2.....	165
Figure 5.5 (a) Ion energy; [b] ion velocity in Zone-2 corresponding to the same conditions as given in Figs. 5.3 and 5.4.....	165

List of Tables

Table 1.1: Table lists typical hydrogen plasma applications, typical sources used along with their respective system and plasma parameters (P : RF or microwave power; p_g : gas pressure; n : plasma density; S : Power density; T_e : electron temperature; L : system length; D : system diameter).....	15
Table 3.1: A gyst of the plasma parameters for different pressures at two axial locations at 650 W microwave power.....	87
Table 3.2: A gyst of the plasma parameters for different pressures at two axial locations and located radially on-axis and towards edge at 650 W microwave power	89
Table 3.3: Ion energies and spread using RFEA at axial locations $z \approx 5$ cm and $z \approx 10$ cm at 650 W microwave power.....	96
Table 4.1: Plasma parameters at axial locations $z \approx -5$ cm, $z \approx 4$ cm and $z \approx 50$ cm at 650 W microwave power.....	113
Table 4.2: Ion energies and spread using RFEA at axial locations $z \approx 5$ cm and $z \approx 10$ cm at 650 W microwave power.....	133
Table 4.3: Table shows the standard deviation of the accuracy for MF1 and MF2.....	137
Table 4.4: Table shows the standard deviation of the accuracy for the two different magnetic field configurations.....	138
Table 4.5: Possible applications of hydrogen plasma with plasma parameters obtained using MF1 and MF2.....	139
Table 4.6: Possible applications of ion beams in hydrogen plasma obtained using MF1 and MF2.....	140
Table 5.1: Model and experimental results comparison at 650 W for MF2.....	166

